Chemical Engineering Journal 106 (2005) 133–143

Chemical Engineering Journal

www.elsevier.com/locate/cej

Local bubble size distributions in agitated vessels

Marko Laakkonen*, Pasi Moilanen, Juhani Aittamaa

Laboratory of Chemical Engineering, Helsinki University of Technology, P.O. Box 6100, FIN-02015 HUT, Finland

Received 7 April 2004; received in revised form 17 November 2004; accepted 23 November 2004

Abstract

Local bubble size distributions (BSD) were measured from 12, 14 and 194 dm^3 agitated vessels with capillary suction probe (CSP) technique. The four investigated systems were air–water, air–aqueous NaCl, air–aqueous starch and CO_2–*n*-butanol. Several gassing rates and stirring speeds were investigated to find their effect on local BSDs. The reproducibility tests and the comparison against photography showed that Sauter mean bubble sizes and volumetric BSDs can be measured accurately from the air–water system with the capillary probe. In the CO_2–*n*-butanol experiments the variation of BSDs with the agitation conditions was reasonable, although the majority of bubbles was likely smaller than the capillary diameter. In the air–water system, bubble size varied more in the Rushton turbine than in the flat-blade turbine (FBT) agitated vessel because of differences in flow fields. The addition of a small amount of NaCl caused a sharp decrease of bubble size in the vicinity of liquid surface. In the impeller discharge flow, bubble size decreased less. The lower coalescence rates due to higher apparent viscosity likely explain the smaller bubbles in the air–aqueous starch system than in the air–water system. In the CO_2–*n*-butanol system, bubbles were notably smaller compared to other systems and the bubble size decreased unexpectedly in the flow from the impeller discharge to the liquid surface. The measured local BSDs are useful for the validation of population balance models that are, as connected to a computational fluid dynamic code, useful tools for the simulation of local mass transfer areas in agitated gas–liquid reactors.

Keywords: Agitation; Bubble size distribution; Capillary technique

1. Background

Agitated gas–liquid vessels are widely used as reactors in many fields of industry. Mass transfer between gas and liquid is a rate limiting step in many stirred tank processes. In large reactors, flow conditions vary often notably. Mass transfer rates are related to mass transfer area, which depends on the local bubble size and gas hold-up. Mass transfer area is obtained most reliably from the bubble size distribution (BSD). Local BSDs can be modelled using population balance models for bubbles as connected to a computational fluid dynamic (CFD) code. Population balance models need validation against local experimental BSDs in order to make them reliable and practical tools for the design and scale-up of agitated gas–liquid reactors [1].

Photography [2–4], phase Doppler anemometry (PDA) [5] and capillary suction probe (CSP) [6–10] are commonly used techniques for the measurement of local BSDs from stirred vessels. During last ten years non-invasive optical techniques have become more popular than capillary technique, since the development of digital cameras, lasers and automatic image processing has made the quantitative optical measurements easier. The accuracy of capillary technique has been criticized in many studies [4,11,12], although optical techniques have weaknesses as well. Manual identification of bubbles from photographs is tedious and computer-aided identification algorithms are uncertain especially with dense dispersions. In contrast to capillary probes, optical techniques require transparent and lean dispersions, which often are industrially less relevant. PDA is an indirect technique with many adjustable parameters. It typically detects the range of 0.005–2.0 mm bubbles, which are assumed to be spherical. Optical techniques also suffer from optical distortions, which may cause bias on the BSDs.

* Corresponding author. Tel.: +358 9451 2642; fax: +358 9451 2694.
E-mail address: marko.laakkonen@hut.fi (M. Laakkonen).

1385-8947/$ – see front matter © 2004 Elsevier B.V. All rights reserved.
doi:10.1016/j.cej.2004.11.010

Nomenclature

BSD	bubble size distribution
d_{32}	Sauter mean bubble diameter (m)
d_i	characteristic bubble diameter of category i (m)
Δd_i	width of bubble size category (m)
d_{max}	maximum detected bubble diameter (m)
d_{min}	minimum detected bubble diameter (m)
FBT	flat-blade turbine
k	consistency index in the viscosity model (kg m^{-1} s^{n-2})
K	calibration coefficient
n	flow index in the viscosity model
N	stirring speed (min^{-1})
N_i	number of bubbles in a size category i
NC	number of discretization categories
p_{calib}	pressure measured after the capillary in a calibration experiment (Pa)
p_{exp}	pressure measured after the capillary (Pa)
PBT	pitched-blade turbine
Q	gas feed rate (m^3 (gas) m^{-3} (dispersion) min^{-1})
RT	Rushton turbine
$v(d_i)$	dimensionless volumetric bubble density of size category i
vvm	gas feed rate (m^3 (gas) m^{-3} (dispersion) min^{-1})
V_{cap}	the sum of bubble volumes calculated by the capillary probe (m^3)
V_{inj}	injected actual gas volume (m^3)

Greek letters

γ	shear rate (s^{-1})
μ_{app}	apparent liquid viscosity (kg m^{-1} s^{-1})

Capillary probes are easier to use and cheaper than optical techniques.

Greaves and co-workers [6–9] have made the main contribution in the development and use of capillary technique for the agitated gas–liquid systems. Recently, Alves et al. [10] used it to investigate local mean bubble sizes in a 0.292 m diameter vessel agitated by two Rushton turbines. A weakness of CSP is that bubbles smaller than the capillary diameter do not convert into slugs and large bubbles may break inside or at the nose of capillary. Kamiwano et al. [13] overcame the former limitation by using a line camera for the detection of bubbles smaller than the capillary diameter. Machon et al. [4] reported that 40% of the overall number of bubbles had diameter between 0.04 and 0.3 mm in a stirred air–water system. By considering this it seems that a major part of the gas–liquid area and gas volume is in the bubbles of size 0.3–6.0 mm, which can be detected by a capillary probe.

There are few systematic studies of local BSDs in agitated vessels. The most extensive is the work of Barigou and Greaves [8]. They measured local BSDs from dense dispersions in a 1 m diameter Rushton turbine agitated vessel and observed a significant spatial spread of BSDs with the measurement position and agitation conditions. Alves et al. [10] compared previous studies and concluded that stirred vessels can be divided roughly into impeller and bulk regions in terms of bubble size. They also noted that the differences in bubble size cannot be attributed to the vessel size, number or type of impellers or measuring method due to large spread of available experimental results. In most studies, mean bubble size has been investigated in few experimental locations using air–water or air–aqueous electrolyte systems. An exception is the work of Schäfer et al. [5] who measured local BSDs in a mixture of silicone oils with PDA from a stirred vessel.

Local BSDs are needed from new gas–liquid systems and vessel geometries to extend and validate population balance models for bubbles. In this work, local BSDs were measured from stirred vessels by varying the vessel size, geometry, operating conditions and chemical system. Capillary technique was used, since it applies to a wide range of agitation conditions. Special attention was paid to the reliability of measured BSDs.

2. Experimental

2.1. Experimental set-up

Local BSDs were measured from the 12, 14 and 194 dm^3 stirred vessels. The 12 dm^3 vessel was a laboratory bioreactor Biostat E manufactured by B. Braun. It included a cooling coil and was agitated by three Rushton turbines (RT). The cooling coil was a 16 mm diameter curved pipe that encased the impeller system at the distance of 40 mm from the vessel wall. Four equally spaced baffles were added to the standard vessel configuration to minimise the vortex at the liquid surface. Gas was distributed to the bottom of vessel through a ring sparger via 21 holes. Main dimensions of the 12 dm^3 vessel are presented in Fig. 1(a). The 14 and 194 dm^3 vessels were geometrically similar and agitated by RTs. They were fully baffled and included also surface baffles to minimise the surface aeration. Gas was distributed through a metal sinter of pore size 15 μm below the impeller to prevent gas jetting at high gassing rates. The dimensions of 14 dm^3 vessel are presented in Fig. 1(b). The corresponding dimensions of 194 dm^3 vessel are obtained from Fig. 1(b) by a multiplication factor 2.423. The BSDs were also measured in a 14 dm^3 vessel agitated by a flat-blade turbine (FBT). These experiments were carried out without surface baffles by distributing the gas through a 0.66 mm tube nozzle (Fig. 1(c)).

The Hydromess® capillary apparatus was used. The experimental set-up is presented in Fig. 2. Gear pump (Ismatec Reglo-Z) with graphite head (2–280 ml min^{-1}) was used to

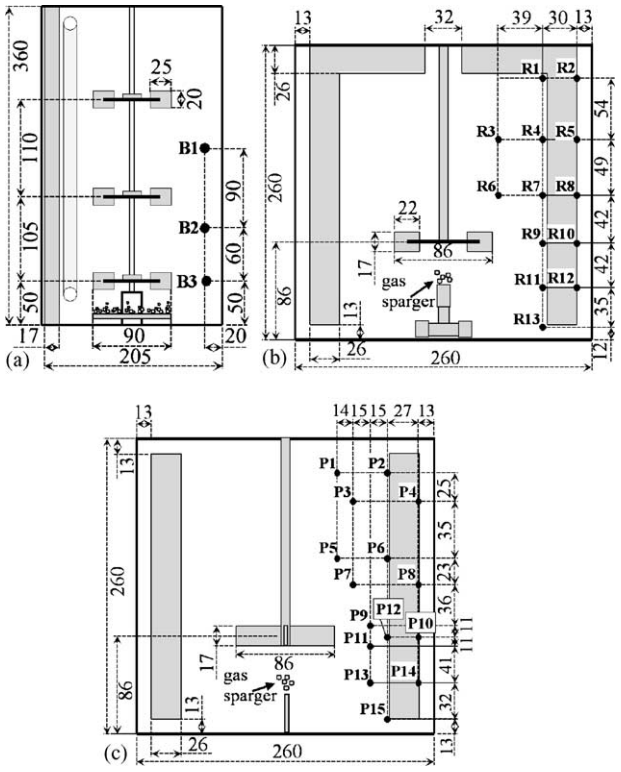

Fig. 1. The experimental points and dimensions of agitated vessels in millimetres: (a) 12 dm^3 bioreactor; (b) 14 dm^3 vessel with Rushton turbine; (c) 14 dm^3 vessel with flat-blade turbine.

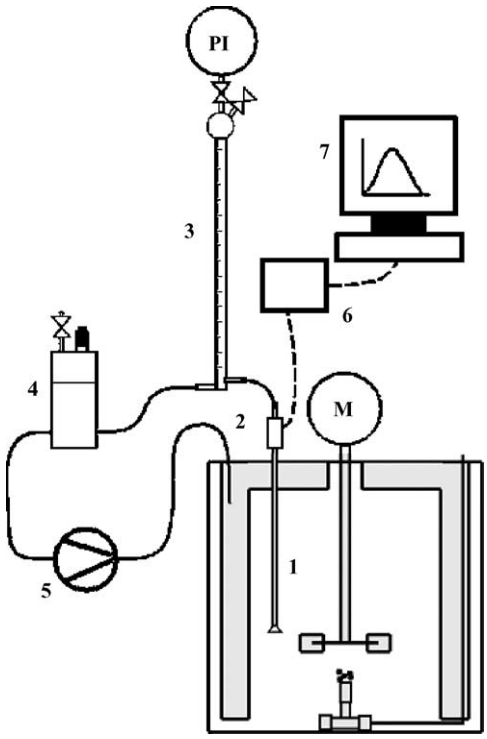

Fig. 2. The experimental set-up: (1) capillary; (2) capillary suction probe; (3) burette for gas separation; (4) pressure equalization tank; (5) gear pump; (6) signal processing unit; (7) computer for data acquisition.

suck the dispersion. Pressure equalisation tank was placed between the pump and the capillary to minimise the velocity fluctuations in the capillary. The funnel-shaped nose of capillary was used to minimise the breakage and coalescence of bubbles at the nose of capillary. Gas was collected after the capillary to a burette that was filled with liquid. A pressure meter was connected to the burette to detect the pressure drop over the capillary. Liquid was recirculated back to the vessel. The experimental points were selected evenly throughout the vessel and are presented in Fig. 1(a)–(c). Experiments were made in the baffle mid-plane. The tangential spread of BSDs was investigated in the point R2 of 194 dm^3 vessel from the air–tap water system. In the 194 dm^3 vessel, the capillary was inserted through the vessel wall to minimise its length and the pressure drop over the capillary.

The capillary inner diameter was selected based on the investigated chemical system and the bubble size. A rule of thumb was that bubbles from one to five times the capillary diameter were detected. To detect the small bubbles, a 0.4 mm capillary was used in the CO_2–*n*-butanol experiments. The large bubbles transformed into long slugs, which were prone to detection errors. Greaves and Kobbacy [6] made a similar observation and explained it with the frequent breakage of bubbles inside the capillary, when bubble size exceeded a critical volume. To eliminate the long slugs and to detect also larger bubbles, 0.8 and 1.2 mm capillaries were used in other experiments (Table 1). About 2000 bubbles were sampled in each experiment.

2.2. Chemical systems and experimental conditions

A summary of experiments is presented in Table 1. The investigated systems were air–water, air–aqueous starch, air–aqueous NaCl and CO_2–*n*-butanol. The experiments were made at laboratory temperature 22 °C and atmospheric pressure. Surface tensions against air were measured with Sigma Tensiometer. The viscosities were measured with Brookfield DV-E viscometer. The starch solutions showed shear-thinning behaviour of viscosity that follows the power law:

$$\mu_{\text{app}} = k\gamma^{n-1} \quad (1)$$

where k is the consistency and n the flow index obtained from the fitting against viscosity measurements. The index values obtained from the fitting for the varying starch concentrations are given in Table 2. As expected, the deviation from Newtonian behaviour increases with the increasing starch concentration.

Surface-active agents and electrolytes are known to decrease bubble size in stirred vessels, since they reduce the tendency of bubble coalescence [4,8,14,15]. For instance, Barigou and Greaves [8] observed a reproducibility problem in the capillary experiments, when the liquid was exposed to the atmosphere for a few days. In our experiments, reproducibility problems due to contamination were minimised by changing the deionised water or *n*-butanol and rinsing the

Table 1
Summary of capillary experiments

System	Vessel size (dm^3)	Impeller type	Measurement points	Gassing rates (vvm)[a]	Stirring speeds (rpm)	Capillary diameter (mm)	Physical properties[b]
Air–deionised water	14	Rushton	R1–R10, R12	0.018, 0.072	260, 340	1.2	$\sigma = 71.6\,mN\,m^{-1}$
	14	Rushton	R1–R13	0.018, 0.072	490	0.8	
	14	Flat-blade	P1–P15	0.018, 0.072	400, 500	1.2	
Air–tap water	194	Rushton	R2, R4, R8, R9, R12	0.018, 0.041	155, 220	1.2	$\sigma = 69.5\,mN\,m^{-1}$
	194	Rushton	R2, R4, R8, R9, R12	0.052	157, 250	0.8	
	194	Rushton	R2, R4, R8, R9, R12	0.072, 0.093	250	0.8	
Air–starch solution	12	3 × Rushton	B1–B3	0.38, 0.67, 0.83, 0.94	400, 600, 800	1.2	$c = 3.0–15.6\,g\,l^{-1}$
	14	Rushton	R2, R3, R6, R8, R9, R12	0.072	260, 340	1.2	$\sigma = 71.5\,mN\,m^{-1}$, $c = 15.6\,g\,l^{-1}$
	14	Rushton	R2, R3, R6, R8, R9, R12	0.29	340	1.2	
Air–NaCl solution	194	Rushton	R2, R9	0.052, 0.072, 0.093	250	0.8	NaCl, 0.87, 8.7, $87\,mmol\,kg^{-1}$
CO_2–*n*-butanol	14	Rushton	R2, R3, R6, R8, R9, R12	0.018, 0.072	260, 340, 380	0.4	$\sigma = 23.5\,mN\,m^{-1}$

[a] vvm = m^3 (gas) m^{-3} (dispersion) min^{-1}.
[b] σ = surface tension, c = starch concentration.

vessels and internals every few days. The effect of contamination was thought to be less significant in the experiments with tap water, aqueous NaCl and starch, since these liquids included solutes. Sodium disulfide (0.1 wt.%) was used as a biocide in the aqueous starch experiments in the 14 dm^3 vessel. The small amount of added electrolyte hardly affected the bubble size, since the starch was of technical grade including many other impurities. Sodium disulfide was not used in the 12 dm^3 vessel, since a new starch solution was prepared every day for the experiments.

The minimum stirring speeds were selected so that the gas was well dispersed. Rushton turbines were used, because they have a wider range of operation than the FBT when dispersing gas. The surface aeration determined the maximum stirring speed. The aim was to eliminate surface aeration, since it cannot be considered accurately as a source term in the stirred tank modelling. Experiments were made at relatively low gas flow rates to enable the comparison against optical techniques presented in the authors' earlier study [16].

Table 2
The parameters of power law viscosity model for aqueous starch solutions at temperature 23 °C

Starch concentration ($g\,l^{-1}$)	Consistency index, k	Flow index, n
3.1	0.00940	0.909
6.1	0.0275	0.853
9.2	0.177	0.481
12.0	0.464	0.487
15.6	1.533	0.355
20.0	1.655	0.354
25.0	2.956	0.384
30.0	6.949	0.324

2.3. Calibration

The capillary apparatus was calibrated for each chemical system and capillary size. A known volume of gas was injected from the calibrated needle and compared to the volume of bubbles given by the capillary apparatus. The calibration coefficients were defined as the ratio of known injected gas volume and the gas volume calculated by the capillary apparatus:

$$K(p_{calib}) = \frac{V_{inj}(1.013\,bar)}{V_{cap}(p_{calib})} \quad (2)$$

The calibration coefficients are smaller than unity, since the slugs expand in the capillary due to pressure drop and the liquid film between the capillary wall and the slug. The calibration coefficients decreased with the decreasing diameter of capillary and with the increasing apparent viscosity of liquid. Bubbles slightly smaller than the capillary diameter transformed into slugs as the gas expanded and the liquid film formed between the slug and the capillary wall. The suction pressure was measured after the capillary and it remained relatively well constant during each experiment. To improve the accuracy of results and to eliminate the effect of varying suction pressure from an experiment to another, the BSDs were calculated with the pressure corrected calibration coefficients obtained from the following equation, which assumes ideal gas.

$$K(p_{exp}) = \frac{p_{exp}}{p_{calib}} K(p_{calib}) \quad (3)$$

The measured calibration coefficients at varying suction pressures showed good agreement with Eq. (3).

2.4. Processing of results

The filtering of raw data was needed to eliminate occasional detection errors caused by the pressure and velocity fluctuations inside the capillary. The capillary probe included two photoelectric sensors. With these sensors, it was possible to determine the suction velocity and the slug length twice for each sampled bubble. The sample was rejected, when slug lengths or suction velocities deviated more than 40%. The calculated BSDs and Sauter mean bubble diameters were not sensitive to this error criterion, although long slugs were rejected at slightly higher probability by using a tight (5%) error criterion. This was expected, since long slugs caused more velocity fluctuations and were more prone to errors than small slugs.

The number of sampled bubbles and the detected bubble size range varied from experiment and chemical system to another. The measured BSDs were made comparable defining dimensionless volumetric densities of bubble size categories as follows:

$$v(d_i) = \frac{d_{\max} - d_{\min}}{\Delta d_i} \frac{N_i d_i^3}{\sum_{j=1}^{\mathrm{NC}} N_j d_j^3} \quad (4)$$

The use of 8–10 bubble size categories (NC) produced smooth BSDs without loosing relevant information. Local Sauter mean bubble diameters d_{32} were calculated as well. The arithmetic mean diameters d_{10} were calculated, but they are likely less reliable due to biasing of number BSDs.

3. Results and discussion

3.1. Reliability of capillary technique

The BSDs measured with the 0.8 and 1.2 mm capillaries were compared at several agitation conditions from the air–deionised water system to check that results are independent on the capillary diameter. The comparison revealed 9% unsystematic maximum error between the 0.8 and 1.2 mm capillaries, which is likely explained by the measurement uncertainty and the contamination of liquid. The reproducibility was checked comparing the BSDs measured at varying agitation conditions from positions R6 and R7 four days apart. The observed deviation was smaller than 10%. Barigou and Greaves [8] reported smaller than 6% reproducibility errors of Sauter mean bubble size, but slightly higher deviation resulted, when liquid was exposed to the atmosphere for few days.

Greaves and Kobbacy [6] pointed out that the sampling rates significantly affect the accuracy of capillary technique and especially the measurement of point-wise gas hold-ups. They observed that 80% of the bubbles behaved in a sample as though a single bubble was sampled whereas the remainder accelerated due the wake effects causing measurement errors. In the present work, the effect of sampling speed was evaluated by comparing measured BSDs at suction speeds 1.0 and 1.5 m s^{-1}. In this range the effect of sampling speed was negligible indicating that the pressure correction (3) compensated the slight changes of suction speed.

The breakage and coalescence of bubbles at the capillary nose affect directly the measured BSDs, but they can be minimised by using a funnel-shaped nose of capillary [7]. Video imaging experiments were made to evaluate their effect on the accuracy of CSP. Although some breakage and coalescence were observed, the majority of bubbles transformed properly into slugs. These phenomena counterbalance each other and their overall effect should be small, when a statistically relevant number of bubbles is sampled. The direction of capillary relative to liquid flow may have some effect on the BSDs as well. On the other hand, this effect cannot be eliminated easily. It was therefore decided to face the nose of capillary to the bottom of vessel in all experiments.

The accuracy of capillary technique was also evaluated by comparing it to the digital imaging in the air–deionised water system. The size of imaged area was about 20 mm × 20 mm close to the tip of the 0.8 mm capillary. The calibration was made by placing a ruler on the imaged region. A large depth of field was used to minimise the biasing of BSDs. About 300 focused bubbles were identified manually from the images to obtain each distribution. The volumetric BSDs from the capillary and photographing experiments are compared in Fig. 3. The agreement is especially good at high gassing rate 0.072 vvm. At low gassing rate 0.018 vvm, the largest observed bubbles were 3.8 mm. A likely reason is the small number of bubbles detected from the photographs. In the CSP experiments, larger bubbles were detected more probably, because 2000 bubbles were sampled. The arithmetic and Sauter mean diameters are compared in Table 3. Both tech-

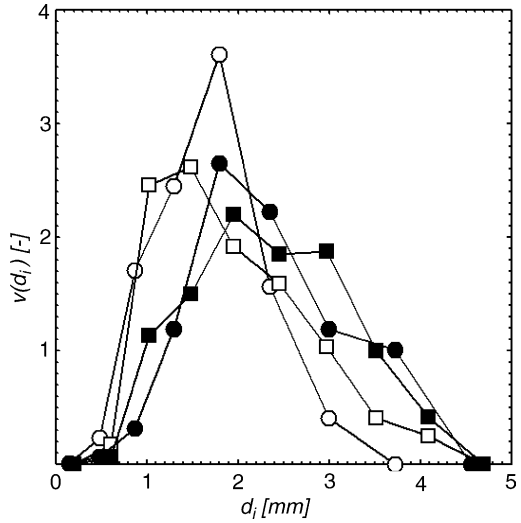

Fig. 3. Comparison of volumetric bubble size distributions measured with digital photography: (◯) Q = 0.018 vvm; (●) 0.072 vvm and with a 0.8 mm capillary probe; (□) Q = 0.018; (■) 0.072 vvm, N = 340 rpm, air–water system, 14 dm^3 vessel.

Table 3
Comparison of measurement techniques, air–deionised water system, point R5 in the Rushton turbine agitated 14 dm^3 vessel

Agitation conditions	Bubble diameter	Capillary (Ø 0.8 mm)	Photography
Q = 0.018 vvm	d_{10}	1.18	0.89
N = 340 rpm	d_{32}	1.61	1.50
Q = 0.072 vvm	d_{10}	1.40	1.24
N = 340 rpm	d_{32}	2.01	2.04

niques give almost equal Sauter mean diameters d_{32} whereas CSP gives larger arithmetic mean diameters d_{10} than photography. The comparison indicates that Sauter mean bubble diameters and volumetric BSDs can be detected accurately from the agitated air–water system with the CSP.

Although the CSP and photographing results agree in the air–water system, a larger deviation was observed in the CO_2–*n*-butanol system [16]. The 0.4 mm capillary seemed to be too large for the detection of CO_2 bubbles and cause a systematic overestimation of bubble size. On the other hand, at high gassing rates bubbles were larger and the volumetric BSDs measured with the CSP and photography agreed better also in the CO_2–*n*-butanol system. Although the BSDs measured from CO_2–*n*-butanol system might be biased, they still show systematic trends with varying agitation conditions. The CSP and photography were not compared in the opaque air–aqueous starch system, but the detected bubbles were only slightly smaller than in the air–water system, which indicates that volumetric BSDs should be accurate.

3.2. Local bubble size distributions

Local volumetric BSDs and Sauter mean bubble sizes in the investigated gas–liquid systems are presented in Fig. 4(a)–(d). Due to a large amount of measured BSDs all results are not presented here, but are available in supplementary material. The results confirm the situation already observed in many previous studies, namely, that bubble sizes vary notably even in laboratory-scale vessels [3–5,8,10,14]. In our experiments, point-wise and spatial variations of bubble size were generally larger than 15% showing systematic trends with varying agitation conditions and experimental locations.

3.2.1. Air–water experiments

The number BSDs were skewed to the left towards small bubble size in all air–water experiments, which agrees with the results of Takahashi and Nienow [3] and Machon et al. [4]. The volumetric BSDs were more symmetrical indicating that the majority of gas volume was in the large bubbles. The BSDs varied most clearly with the measurement point in the air–tap water experiments in the 194 dm^3 vessel. This was expected, since bubbles have more time to coalesce and the differences between experimental points become more pronounced, when mixing time is longer. At all experimental conditions, bubbles were smallest in the impeller discharge in the point R9 (Fig. 4(b)). The largest bubbles were observed in the points R4 and R12. The bubble size increased in these points with the increasing stirring speed while it decreased in the points R2, R8 and R9. Reduced coalescence rates due to slight contamination or lean dispersion could explain the decrease of bubble size at regions far from the impeller (R2, R8). Barigou and Greaves [8] observed the decrease of Sauter mean bubble diameter with the increasing stirring speed only in the impeller discharge flow. It appears that due to higher gas hold-up the coalescence had a more important role in controlling the bubble size in regions far from the impeller in their experiments than in our work. Alves et al. [10] measured local bubble sizes with the capillary technique and reported that coalescence was mostly completed as the flow of dispersion from the Rushton turbine reaches the wall, although some coalescence may still occur in the upward or downward flow near the wall.

The effect of stirring speed on local Sauter mean bubble size in the 14 dm^3 Rushton turbine agitated vessel is presented in Fig. 5. The power requirements of agitation were calculated using the power numbers obtained from the measured torques on impeller in a geometrically similar 194 dm^3 vessel. The use of measured power numbers from a larger vessel was motivated by the fact that power measurements are inaccurate in a small vessel due to a small torque. It was further assumed that the impeller power number should be relatively independent on the vessel size at low gassing rate, if the vessels are geometrically similar and the scale-up ratio is small.

As can be concluded from Fig. 5, the effect of stirring speed is complicated. At low stirring speed, bubbles are smaller in the central region (R3, R6, R11, R13) than close to the wall (R2, R5, R8, R12). At higher stirring speed, contrary behaviour is observed above the impeller. Below the impeller, dispersion becomes more homogeneous when stirring speed is increased. Bubble size decreases with the increasing stirring speed in the impeller discharge flow (R9), but also close to the wall (R5, R8) and near the liquid surface (R1, R2). This agrees with the air–tap water experiments in the 194 dm^3 vessel. The bubble size increases with the increasing stirring speed in the central region above the impeller (R3, R4, R7) and below the impeller (R11, R13). The better recirculation of bubbles and the surface entrainment of gas in the point R3 are probable explanations. In the points R6, R10 and R12 mean bubble size has a maximum with the increasing stirring speed (Fig. 5). The better recirculation explains the initial increase of bubble size as higher gas hold-up promotes the bubble coalescence. The further decrease of bubble size is likely related to the changes in the flow field and the increased intensity of turbulence.

Tangential variation of BSDs was investigated close to the liquid surface in the point R2 of 194 dm^3 vessel at several agitation conditions. The variation of BSDs with the tangential location was clear and is presented in Fig. 6. The results confirm the observations of Barigou and Greaves [8], namely, that bubbles are notably smaller in the windward side than

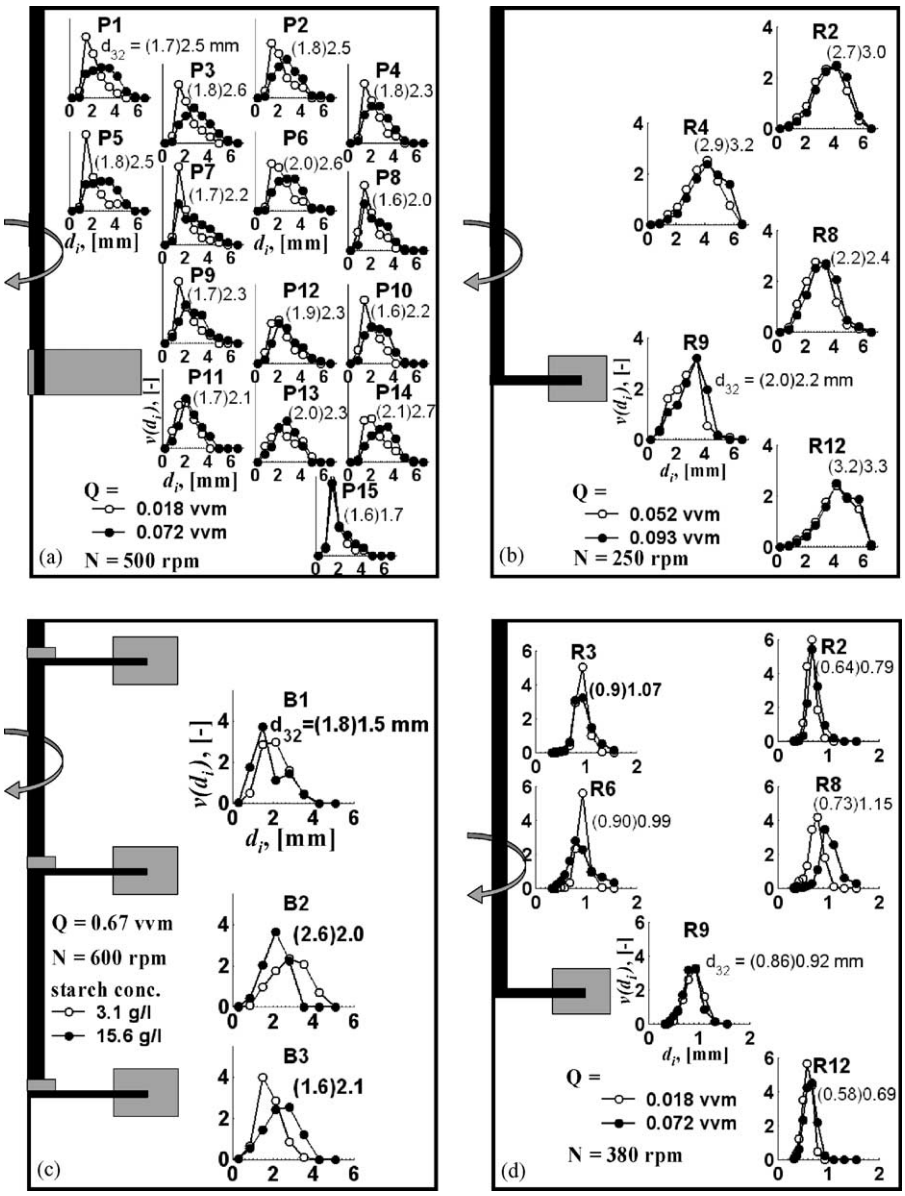

Fig. 4. Local volumetric bubble size distributions and Sauter mean diameters (d_{32} in parentheses corresponds BSD with open markers): (a) air–deionised water, 14 dm^3 vessel; (b) air–tap water, 194 dm^3 vessel; (c) air–aqueous starch, 12 dm^3 bioreactor; (d) CO_2–*n*-butanol, 14 dm^3 vessel.

in the leeward side of the baffle. It should be noted that baffles were connected to the wall in their experiments, which differs from our geometry where baffles were at a small distance from the wall. Barigou and Greaves [8] explained their observations with a more intense turbulence field in front of baffle. Also, the lower pressure caused by the fluid motion leads to the accumulation of gas behind the baffles promoting the coalescence. The BSDs in Fig. 6 show that bubbles are larger in the baffle mid-plane (R2) than in the windward side of baffle. This agrees with the results of Barigou and Greaves [8]. They observed significantly larger bubbles in the baffle mid-plane than in the baffle plane. Surprisingly, bubbles are small in the point marked with open circle in Fig. 6. The complex three-dimensional flow such as secondary circulations loops close to the liquid surface as suggested by Nienow et al. [17] could explain the strong tangential variation.

The bubble size distributions varied less in the RT than FBT agitated 14 dm^3 vessel. The smaller power number of FBT was compensated by using higher stirring speeds (Table 1) and should not explain the deviation. The bubble size decreased with the increasing stirring speed and with the decreasing gassing rate in all experimental points (P1–P15) (Fig. 4(a)). The visual observation showed that FBT produced a downward axial flow from the impeller. As a consequence, some primary bubbles reached the impeller only through circulation. Also, the single nozzle distributor produced fluctuating bubble trails and jetting at high gassing rates. The flow

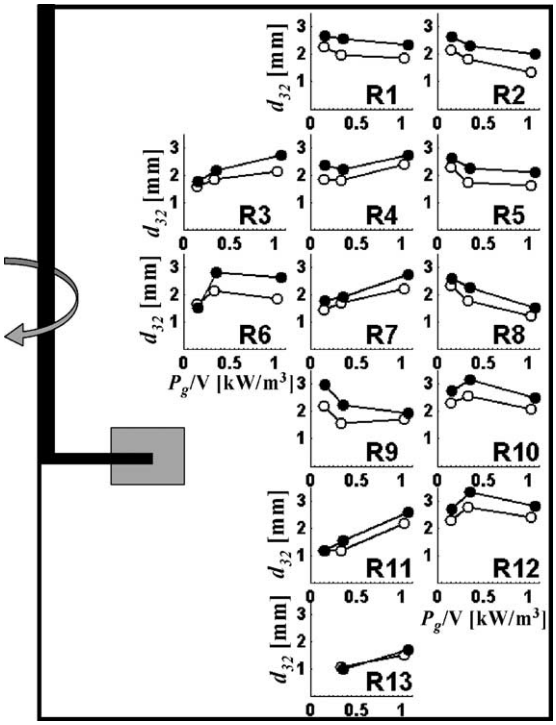

Fig. 5. Local Sauter mean bubble sizes vs. agitation power, air–deionised water: (◯) $Q = 0.018$ vvm; (●) 0.072 vvm, 14 dm^3 vessel agitated by Rushton impeller.

field likely explains the moderate spatial variation of BSDs compared to the experiments with RT. Schäfer et al. [5] made a similar observation, when they measured local bubble sizes with PDA in a vessel agitated by RT and PBT. In their experiments, the radial jet generated by the RT prevented the rise of large bubbles from the lower to the upper flow region close to the vessel wall, which resulted into larger bubbles in the circulation loop below the impeller. The PBT, instead, generated only one large eddy, which allowed the large bubbles to rise more freely.

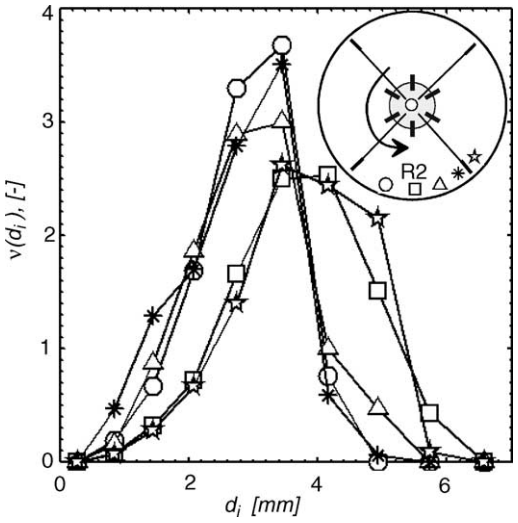

Fig. 6. Tangential variation of volumetric bubble size distributions, point R2 in the 194 dm^3 vessel, air–tap water, $Q = 0.093$ vvm, $N = 250$ rpm.

3.2.2. Air–aqueous NaCl experiments

The electrolytes have been suggested to form an electrical double layer in the liquid film, which immobilizes bubble interface reducing the tendency of bubble coalescence (e.g. [18]). Lessard and Zieminski [19] observed that bubble size is related to the valency of ions. A small concentration of higher valency electrolyte such as $MgCl_2$ caused a similar effect as a higher concentration of low valency electrolyte such as NaCl.

The controlling mechanisms of bubble size were studied by measuring BSDs from dilute NaCl solutions close to the liquid surface (R2) and in the impeller discharge flow (R9). The added amounts of NaCl were 0.87, 8.7, 87 mmol kg^{-1} and significantly lower than the critical concentrations at which the rate of coalescence has been reported to be 50% of the pure water [19]. The BSDs were measured at several gassing rates. Although the added amounts of NaCl were small, the deviation from the BSDs in tap water was significant and is illustrated in Figs. 7(a) and (b). The first addition of NaCl caused a sharp decrease of bubble size and further additions decreased bubble size moderately. The relative effect of adding salt is larger close to the liquid surface (R2) than in the impeller discharge flow (R9). This indicates that bubble size is controlled by the breakage in the impeller discharge flow and by the coalescence in the regions far from the impeller. This agrees with the observations of Barigou and Greaves [8].

3.2.3. Air–aqueous starch experiments

In the viscous air–aqueous starch (15.6 g l^{-1}) system, bubbles were slightly smaller than in the air–water system in the 14 dm^3 agitated vessel (Fig. 8). Manikowski et al. [20] made a similar observation. In their experiments, the number of small bubbles increased progressively with the increasing viscosity in aqueous carboxy-methyl cellulose systems in a 200 dm^3 vessel agitated by multiple impellers. At the same time, large bubbles increased in size resulting into bimodal BSDs. The BSDs were occasionally bimodal also in our experiments,

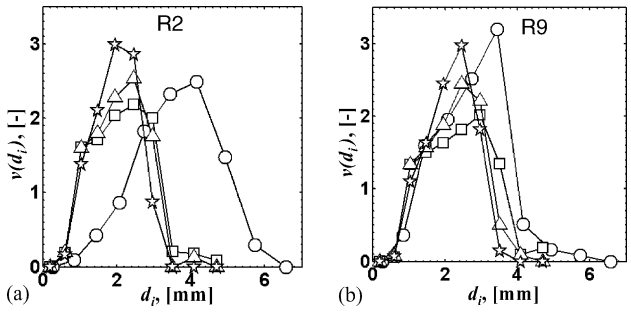

Fig. 7. Local volumetric bubble size distributions, air–aqueous NaCl: (◯) 0.0 mmol kg^{-1}; (□) 0.87 mmol kg^{-1}; (Δ) 8.7 mmol kg^{-1}; and (☆) 87 mmol kg^{-1} NaCl, 194 dm^3 vessel (a) in the vicinity of liquid surface (R2) and (b) in the impeller discharge flow (R9), $Q = 0.052$ vvm, $N = 250$ rpm.

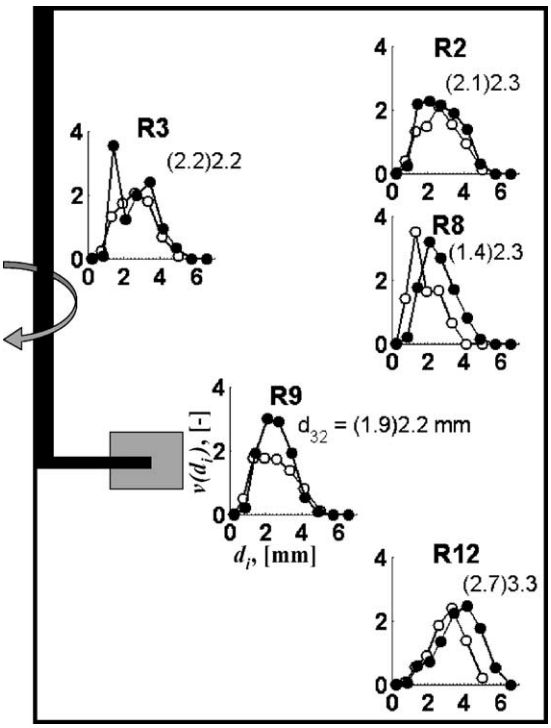

Fig. 8. Local volumetric bubble size distributions Sauter mean bubble diameters in the (●) air–deionised water and (○) air–aqueous starch (15.6 g l^{-1}) solution (d_{32} in parentheses) in the 14 dm^3 vessel (Q = 0.072 vvm, N = 340 rpm).

but systematic trend was not observed. Andrews [21] has proposed that the lower coalescence rates could explain the smaller bubbles in viscous fluids. On the other hand, the lower coalescence rates are counterbalanced by the higher viscous stresses that resist the bubble breakage. The inhibition of coalescence due to sodium disulfide (biocide) and other impurities in the starch are other reasons for the smaller bubble size. In the 12 dm^3 bioreactor, bubble size decreased with the increasing viscosity (i.e. concentration of starch) in the point B1 and increased in the point B3 whereas systematic trend was not observed in the point B2. Visual observation revealed a slight compartmentalisation of gas, which agrees with the observations of Manikowski et al. [20]. The changes in liquid viscosity affect the interactions between bubbles and also the flow field making its overall effect on local BSDs complicated. This could explain, why systematic changes of local BSDs were not observed in the 14 dm^3 vessel (Fig. 8) or in the 12 dm^3 bioreactor (Fig. 4(c)). The presence of cooling coil further complicated the flow field making the evaluation of local trends in the 12 dm^3 bioreactor difficult.

Although the bubble sizes varied complicatedly with the measurement point and viscosity, the effects of gassing rate and stirring speed were clear. The bubble size decreased with the increasing stirring speed and with the decreasing gassing rate in almost all experimental points in both 12 and 14 dm^3 vessels. A noticeable exception was the decrease of bubble size in the point R12 as the gassing rate increased from 0.072 to 0.29 vvm in the 14 dm^3 vessel. The flooding caused by the decreased pumping capacity of impeller could explain this.

3.2.4. CO_2–*n*-butanol experiments

Bubbles were notably smaller in the CO_2–*n*-butanol than in the air–water system (Fig. 4(d)). The small CO_2-bubbles follow the liquid better, which resulted into a more homogeneous dispersion compared to other investigated systems. The low surface tension (23.5 mN m^{-1}) promotes the bubble breakage leading to smaller bubble sizes. *n*-Butanol is also slightly more viscous than water, which reduces the bubble coalescence. Furthermore, the dissolved CO_2 may decrease the tendency of bubble coalescence as Takahashi et al. [2] have observed. In their experiments, Sauter mean bubble diameter decreased 10%, when water was saturated with CO_2.

Bubbles size decreased from the tip of impeller to the wall and the liquid surface through points R9, R8 and R2 at gassing rate 0.018 vvm (Fig. 4(d)). At higher gassing rate 0.072 vvm, bubbles were larger in the point R8 than in the points R9 or R2. The lower accuracy of CSP in the CO_2–*n*-butanol system could explain the unexpected result [16]. On the other hand, Machon et al. [4] observed similar dependence on the measurement point, when BSDs were investigated in electrolyte and alcohol solutions in the 2.65 dm^3 stirred vessel with photography. Stirring speed was 770 rpm and gassing rate ~0.88 vvm in their experiments. Machon et al. [4] suggested that the level of turbulence is high enough to cause the bubble breakage also far from the impeller. This seems reasonable, since their vessel was small and the stirring speed high. Also Schäfer et al. [5] observed larger bubbles in the impeller discharge flow than elsewhere in the vessel. They suggested that the large primary bubbles from the gas distributor or the trailing gas vortices in the impeller discharge flow result into larger bubble size in the impeller region. This could also explain our observations. The dissolution of CO_2 is another reason for the decrease of bubble size from the impeller towards the liquid surface, but this seems not probable as the *n*-butanol was continuously gassed and was likely saturated with CO_2.

Similarly as in other investigated systems, bubble size increased with the increasing gassing rate throughout the vessel (Fig. 4(d)). The results not shown here (available in supplementary material) revealed the decrease of bubble size with the increasing stirring speed elsewhere but in the points R6 and R12 at Q = 0.018 vvm. The better recirculation of bubbles explains the increase of bubble size in the points R6 and R12. The effect was not, however, as clear as in air–water system, since small CO_2 bubbles follow liquid better even at low stirring speeds.

4. Conclusions

Local bubble size distributions were measured from mechanically agitated gas–liquid dispersions with the capillary suction probe technique. The reproducibility tests and the

comparison against photography showed that Sauter mean bubble sizes and volumetric BSDs were detected accurately from the air–water system. The measured BSDs showed reasonable variation also in the CO_2–*n*-butanol system, although the majority of bubbles seemed to be smaller than the capillary diameter of 0.4 mm.

The BSDs showed more significant spatial variation with the Rushton turbine than with the flat-blade impeller, which is likely explained by the differences in flow fields. The systematic variation of BSDs was observed in the air–water experiments in both 14 and 194 dm^3 vessels. The bubble size increased with the increasing stirring speed in the regions of downward flowing liquid and decreased in the impeller discharge flow and in the regions upward flowing liquid. The effect of increasing the gassing rate was to increase the bubble size throughout the vessel. Even a small amount of NaCl caused a sharp decrease of bubble size in the vicinity of liquid surface in the 194 dm^3 vessel. In the impeller discharge flow, bubble size decreased less. This indicates that the breakage controls the bubble size in the impeller region and the coalescence in the bulk region of vessel in 'pure' systems and even a small amount of NaCl suppresses the coalescence. The reduced coalescence rates due to higher viscosity seem to explain the slightly smaller bubbles in the air–aqueous starch compared to the air–water system in the 14 dm^3 vessel. In the CO_2–*n*-butanol system, bubble size decreased from the impeller discharge to the liquid surface, which was unexpected, but is in line with some earlier studies [4,5].

Capillary technique has many benefits despite the fact that bubbles smaller than the capillary diameter are not detected. Compared to optical techniques such as photography or phase Doppler anemometry, it applies to dense and opaque dispersions, requires no transparent vessels and is also cheap and easy to use. On the other hand, a superior technique is not available at the moment, and various techniques should be used to complement each other. Among others capillary probes are useful for the investigation of local BSDs from stirred vessels. They also seem to be a good choice when local gas–liquid mass transfer areas are of interest, since the bubbles detected by the capillary include a significant fraction of the gas–liquid surface area and gas volume. The measured local BSDs are useful for the validation of population balance models, which can be connected to computational fluid dynamic programs and used to study local mass transfer area in agitated gas–liquid reactors.

Acknowledgements

The authors want to thank Asta Nurmela, B.Sc. and Juha Jokila, M.Sc. for carrying out the capillary experiments. Financial support from the Graduate School of Chemical Engineering (GSCE) and KaNeMa project, that is a part of the Multiphase and Industry (MANDI) program coordinated by National Technology Agency of Finland (TEKES) is acknowledged.

Appendix A. Supplementary data

Supplementary data associated with this article can be found, in the online version, at doi:10.1016/j.cej.2004.11.010.

References

[1] V.V. Ranade, Computational Flow Modeling for Chemical Reactor Engineering, Academic Press, San Diego, USA, 2002, p. 443.
[2] K. Takahashi, W.J. McManamey, A. Nienow, Bubble size distributions in impeller region in a gas-sparged vessel agitated by a Rushton turbine, J. Chem. Eng. Jpn. 25 (4) (1992) 427–432.
[3] K. Takahashi, A.W. Nienow, Bubble sizes and coalescence rates in an aerated vessel agitated by a Rushton turbine, J. Chem. Eng. Jpn. 26 (5) (1993) 536–542.
[4] V. Machon, A.W. Pacek, A.W. Nienow, Bubble sizes in electrolyte and alcohol solutions in a turbulent stirred vessel, Chem. Eng. Res. Des. 75A (1997) 339–348.
[5] M. Schäfer, P. Wächter, F. Durst, Experimental investigation of local bubble size distributions in stirred vessels using Phase Dobbler Anemometry, in: H.E.A. van den Akker, J.J. Derksen (Eds.), Proceedings of the 10th European Conference on Mixing, Elsevier, Delft, The Netherlands, 2000, pp. 205–212.
[6] M. Greaves, K.A.H. Kobbacy, Measurement of bubble size distribution in turbulent gas–liquid dispersions, Chem. Eng. Res. Des. 62 (1984) 3–12.
[7] M. Barigou, M. Greaves, A capillary suction probe for bubble size measurement, Meas. Sci. Technol. 2 (1991) 318–326.
[8] M. Barigou, M. Greaves, Bubble-size distributions in a mechanically agitated gas–liquid contactor, Chem. Eng. Sci. 47 (8) (1992) 2009–2025.
[9] M. Barigou, M. Greaves, Bubble size in the impeller region of a Rushton turbine, Chem. Eng. Res. Des. 70 (1992) 153–160.
[10] S.S. Alves, C.I. Maia, J.M.T. Vasconcelos, A.J. Serralheiro, Bubble size in aerated stirred tanks, Chem. Eng. J. 3990 (2002) 1–9.
[11] A.W. Pacek, A.W. Nienow, Measurement of drop size distribution in concentrated liquid–liquid dispersions: video and capillary techniques, Chem. Eng. Res. Des. 73 (1995) 512–517.
[12] T. Martin, Gas Dispersion with Radial and Hydrofoil Impellers in Fluids with Different Coalescence Characteristics, Herber Utz Verlag Wissenschaft, Munchen, 1996, p. 240.
[13] M. Kamiwano, M. Kaminoyama, K. Nishi, D. Shirota, A method for measuring bubble diameter distribution in gas–liquid agitated vessel under high gas hold-up using real-time high-speed image processing system, J. Chem. Eng. Jpn. 31 (8) (1998) 366–373.
[14] P.H. Calderbank, Physical rate processes in industrial fermentation. Part 1. The interfacial area in gas–liquid contacting with mechanical agitation, Chem. Eng. Res. Des. 36 (1958) 443–463.
[15] R. Parthasarathy, G.J. Jameson, N. Ahmed, Bubble breakup in stirred vessels—predicting the Sauter mean diameter, Chem. Eng. Res. Des. 69 (1991) 295–301.
[16] P. Moilanen, M. Laakkonen, J. Aittamaa, Measurement of local bubble size distributions in stirred vessels using various techniques, in: Proceedings of the AIChE Annual Meeting, San Francisco, 16–21 November 2003.
[17] A.W. Nienow, D.J. Wisdom, J.C. Middleton, The effect of scale and geometry on flooding, recirculation, and power in gassed stirred vessels, in: H.S. Stephens, J.A. Clarke (Eds.), Proceedings of the 2nd European Conference on Mixing, BHRA Fluid Engineering, England, 1977, Paper F1.

[18] R.V. Chaudari, H. Hoffmann, Coalescence of gas bubbles in liquids, Rev. Chem. Eng. (1994) 131–190.
[19] R.R. Lessard, S.A. Zieminski, Bubble coalescence and gas transfer in aqueous electrolytic solutions, Ind. Eng. Chem. Fundam. 10 (1971) 260–269.
[20] M. Manikowski, S. Bodemeier, A. Luebbert, W. Bujalski, A.W. Nienow, Measurement of gas and liquid flow in stirred tank reactors with multiple agitators, Can. J. Chem. Eng. 72 (5) (1994) 769–781.
[21] S.P.S. Andrews, Gas–liquid mass transfer in microbiological reactors, Chem. Eng. Res. Des. 60 (1982) 3–10.